

## 7. ASTROMETRIC ANALYSIS OF TRANSIT DATA

*Tycho astrometric data processing is described, leading from the transit times to a geometric calibration of the slit system and to the astrometric parameters of the Tycho stars. Special quality parameters were derived for the astrometric solution of each star, in addition to the conventional internal standard errors.*

---

### 7.1. Theoretical Basis of the Astrometric Reduction

---

#### **Input Data**

The purpose of the reductions in Tycho astrometry processing is to determine the five astrometric parameters (i.e. the position and proper motion components and the parallax) for each Tycho star for which a sufficient number of observations (the ‘identified transits’, see Section 7.2 or Chapter 6) have been collected. This work combines the following information:

- (i) transit times, i.e. the observed instants at which the stars cross one of the fiducial reference lines on the focal surface of the telescope (the output of the ‘detection’ processing, described in Chapters 2 and 4);
- (ii) attitude data, describing the celestial pointing of the satellite, i.e. the coordinates of the viewing directions, as a function of time (as determined by the main mission data processing, Volume 3, Chapter 7). The attitude was supplied by NDAC, and included in the predicted transit times, as described in Chapter 6;
- (iii) star mapper calibration data, which describe the geometry of the fiducial reference lines on the grid with respect to the viewing directions, assembled from laboratory measurements of the grid and further corrections derived in the course of the astrometry task itself. These corrections were related to the transit times, the attitude and the grid in such a way that the Tycho reference system of positions was tied directly to the Hipparcos reference frame, as explained below;
- (iv) the Tycho Input Catalogue (TIC) of 3 million stars derived from ground-based catalogues;
- (v) the Hipparcos catalogue of positions, proper motions and parallaxes.

Broadly speaking, each identified transit observation defined a position line for the star, namely the projection onto the celestial sphere of the fiducial line (the centre line of the four slits) at the time of the star’s transit. This projection could be calculated from the

attitude and the grid calibration data. The intersection of several such position lines provided the astrometric position of the star, and its variation with time allowed the determination of the proper motion and parallax. In practice, a least-squares solution was made for the astrometric parameters, using linearized coordinates within a small field around the expected position. This expected position was taken from the Tycho Input Catalogue of 3 million stars (Chapter 3) in a first stage of data reduction, and from the Tycho Input Catalogue Revision of one million stars (Chapter 5) in the final processing.

It is worth noting that in principle the Tycho data reduction could have been started without an input catalogue of positions of real stars; a uniform net of about 200 000 starting positions per square degree could have been used. But the use of the much smaller Tycho Input Catalogue has greatly facilitated the data reduction. The resulting limiting magnitude in the final catalogue is fainter: without any input catalogue the acceptance limit for the signal-to-noise ratio of transits and of stars would have to be higher lest the false transits and false stars be too numerous. A ‘false star’ would be the result of a purely random concentration of position lines at a point on the sky.

### Star Mapper Geometry

The star mapper grid consisted of eight slits arranged in two groups: the vertical group ( $g = 1$ ) and the chevron or inclined group ( $g = 2$ ). The field coordinates ( $w, z$ ) represent direction cosines with respect to the orthogonal axes  $\mathbf{w}$  and  $\mathbf{z}$  as defined in Figure 1.1. For the present task the individual slits are not of particular relevance, but only the ‘fiducial line’ of each group. This line can be thought of as the centre of gravity of the four slits in a group, taken along the scanning (or  $w$ ) direction. The fiducial lines are defined, in field coordinates, by means of the equation:

$$w = w_{fg}^*(z) + \Delta w_g(z) \quad (f = \pm 1, \quad g = 1, 2) \quad [7.1]$$

where  $f = +1$  is the index for the preceding field of view of satellite rotation, and  $f = -1$  for the following field on the sky.  $\Delta w_g(z)$  is the tabulated ‘medium-scale irregularity’ derived at first from laboratory measurements of the grid. The functions  $w_{fg}^*(z)$  and corrections to the medium-scale irregularities were obtained from grid calibration by means of in-orbit observations (Section 7.3). The following representation was used:

$$w_{f1}^*(z) = (h + h_{11}z) f + w_{10} + w_{11}z \quad [7.2a]$$

$$w_{f2}^*(z) = (h + h_{21}^+z) f + w_{20} + w_{21}^+z + h_f \quad \text{if } z > 0 \quad [7.2b]$$

$$= (h + h_{21}^-z) f + w_{20} + w_{21}^-z - h_f \quad \text{if } z < 0 \quad [7.2c]$$

with Equation 7.2(a) valid for the vertical slit group, Equation 7.2(b) for the upper branch of the chevron group and Equation 7.2(c) for the lower. Apart from the terms  $\pm h_f$ , which are explained below, this representation is very similar to the one used for the attitude determination by the NDAC Consortium (Lindgren *et al.* 1992, and Volume 3, Chapter 10). Nominally, the star mapper slits are straight lines in the ( $w, z$ ) plane, with the two branches of the chevron meeting exactly at  $z = 0$ . For the preceding star mapper grid, the one shown in Figure 1.1, the nominal values of the 11 geometric parameters are:  $h, h_{11}, h_{21}^+, h_{21}^-, h_{-1}, h_{+1}, w_{11} = 0, w_{21}^+ = -1, w_{21}^- = +1, w_{10} \simeq 0.00938$  and  $w_{20} \simeq 0.01545$ ; all signs are reversed for the (redundant) star mapper on the opposite side of the main grid (the following star mapper grid), which was however never used.

The parameter  $h$  accounts for any deviation of the actual basic angle between the two fields of view on the sky from the adopted constant value  $\gamma$ , which is  $58^\circ$ . The terms  $h_{-1}$  (for the following field) and  $h_{+1}$  (preceding field) correspond to small shifts, in the  $z$  direction, of the image centroids as defined by the transit times. As mentioned above, these shifts are by definition zero in the attitude determination process. In Tycho astrometry, however, a slightly different centroid definition had to be expected due to the use of different algorithms, resulting in non-zero shifts, by a fraction of an arcsec. A similar shift in the  $w$  direction was absorbed by the parameters  $w_{10}$  and  $w_{20}$ .

The parameters  $w_{gk}$  in Equation 7.2 represent zero-points and inclinations of different parts of the slits, and the calibration gives corrections to the parameter values used in predicting the group crossing times. Only zero and first order calibration parameters were used. Second and higher order terms, representing curvature, were assumed constant over the mission and as such absorbed in a table of ‘medium scale irregularities’, discussed in Section 7.3.

A set of calibration parameters was derived from an observation period of about 24 hours, usually defined by the length of observation time contained on one tape delivered by ESOC. These parameters, suitably interpolated by splines, were used to correct the observed transit times when astrometric parameters of the stars were subsequently derived. The calibration parameters were constant over much longer stretches of time (except for e.g.  $w_{10}$  at times of refocussing), but it was decided that practically nothing could be gained by smoothing over greater lengths of time than a few days (see Section 7.3).

In the actual Tycho astrometric processing the calibration parameters were always determined as small corrections to the corresponding parameters used in the NDAC star mapper processing, since the NDAC parameters were used in the prediction updating processing (Chapter 6) together with the NDAC attitude.

### Observation Equations

The observation equations are given here, with their mathematical relation to the star mapper geometry and the astrometric parameters. The relation to the satellite attitude and to the celestial coordinates of the stars is described in Chapter 4 of this volume and in Section 1.2 of Volume 1.

All calculations of celestial directions were made in a single, well-defined coordinate system which coincided to better than 0.1 arcsec with the final system in which the Tycho Catalogue is published (the Hipparcos reference frame, which is the optical representation of the International Celestial Reference System, ICRS). At the end of the Tycho reductions all positions and proper motions were transformed, by a rigid rotation of the coordinate axes, to conform as closely as possible with the Hipparcos reference frame. Since the observations were completely decoupled from the rotation of the Earth, the effects of precession and nutation did not appear in any of the data reduction calculations.

Consider now the computation of the astrometric parameters. Let  $(w, z)$  be the field coordinates and  $f$  as defined above for an object observed at instant  $\tau$ . The object’s distance from the fiducial line of slit group  $g$  is defined as:

$$u(\tau) = w(\tau) - (w_{fg}^*(z) + \Delta w_g(z)) \quad [7.3]$$

The crossing time or transit time of the fiducial reference line for the grid is given by the equation  $u(\tau) = 0$ . The observations consist of measured transit times  $\tau_{\text{obs}}$  associated with a specific object.

The five astrometric parameters for star  $i$  are  $\alpha_i$ ,  $\delta_i$ ,  $\pi_i$ ,  $\mu_{\alpha_i}$ , and  $\mu_{\delta_i}$ . They were determined by a least-squares solution from the on average 130 observed transit times of a star. The solution is closely linked to the determination of (improved) grid parameters ( $h, w_{10}, \dots$ ) and the formulation below takes full account of this calibration.

For each observed transit  $\tau_{\text{obs}}$  of star  $i$  on slit group  $g$ , the following observation equation can be set up:

$$\begin{aligned} & \frac{\partial u}{\partial \alpha_i} \Delta \alpha_i + \frac{\partial u}{\partial \delta_i} \Delta \delta_i + \frac{\partial u}{\partial \pi_i} \Delta \pi_i + \frac{\partial u}{\partial \mu_{\alpha_i}} \Delta \mu_{\alpha_i} + \frac{\partial u}{\partial \mu_{\delta_i}} \Delta \mu_{\delta_i} \\ & + \frac{\partial u}{\partial h} \Delta h + \frac{\partial u}{\partial h_{11}} \Delta h_{11} + \dots + \frac{\partial u}{\partial h_{+1}} \Delta h_{+1} \\ & + \text{noise} = u_{\text{obs}} - u_{\text{calc}} \end{aligned} \quad [7.4]$$

where  $u_{\text{obs}} = 0$  at time  $\tau_{\text{obs}}$  by definition, while  $u_{\text{calc}}$  is the distance calculated (predicted) from the current values of the astrometric parameters (typically the position in the Tycho Input Catalogue Revision), current grid calibration parameters, and the attitude.  $\Delta \alpha_i, \dots, \Delta h_{+1}$  are the corrections to these current parameters, to be determined by the least-squares method.

The predicted distance at time  $\tau_{\text{obs}}$  of a star from the fiducial reference line of the slit group, measured along the direction of motion, corresponds to a predicted transit time  $\tau_{\text{calc}}$ , which is related to  $u_{\text{calc}}$  through the velocity  $v_{\text{scan}}$  of the stellar image relative to the grid.  $v_{\text{scan}}$  is negative at the nominal direction of spin of the satellite  $v_{\text{scan}} = du/dt \simeq -8.18 \times 10^{-4} \text{ rad s}^{-1}$ . It is noted that the velocity component in the  $z$ -direction is relatively small, but must be taken into account. It follows that:

$$\Delta u \equiv u_{\text{obs}} - u_{\text{calc}} = -v_{\text{scan}} (\tau_{\text{obs}} - \tau_{\text{calc}}) \quad [7.5]$$

is the right-hand side of Equation 7.4.

The observation, Equation 7.4, is given in spherical coordinates, whereas a formulation using relative tangential coordinates in the vicinity of each Tycho Input Catalogue position was used in practice, thus simplifying the data reduction to a linear problem.

The uncertainty,  $\sigma_u$ , of the right-hand side of Equation 7.5 depended on two major error sources, contained in the last two terms: photon-statistical uncertainty of the observed transit time (converted to arcsec along scan),  $\sigma_\tau$ , and the attitude uncertainty. Considering the way in which the attitude was determined, it was reasonable to assume that the attitude errors in the calculated ( $w, z$ ) were uncorrelated and characterized by nearly constant standard deviations  $\sigma_w, \sigma_z$ . Then, to sufficient accuracy:

$$\sigma_u^2 = \sigma_\tau^2 + \sigma_w^2 + (g-1)\sigma_z^2 \quad [7.6]$$

where  $g-1 = 0$  for the vertical group and  $= 1$  for the chevron group, according to the definition of  $g$ .

The photon-statistical error  $\sigma_\tau$  was calculated for each transit at a slit group as a function of the estimated star and background count rates (and measured in arcsec along the scan).  $\sigma_w$  and  $\sigma_z$  are functions of time. Their average values determined from observations were about  $\sigma_w = 7 \text{ mas}$  and  $\sigma_z = 35 \text{ mas}$  which was very satisfactory since at least  $\sigma_z = 50 \text{ mas}$  error was expected for the inclined slits before launch (see Table 11.1

in Høg 1989). In practice a slightly different formulation than Equation 7.6 was used in order to accomodate variations during the mission (Equation 11.3).

Dividing Equation 7.4 by the estimated standard deviation from Equation 7.6 gives an observation equation of unit weight. Let us assume that the grid calibration requires, for a short period of the mission, a total of  $N_c$  parameters. The  $k$ -th observation equation can then be written in matrix form:

$$\mathbf{B}_k \Delta \mathbf{a}_{i(k)} + \mathbf{C}_k \Delta \mathbf{c} + v_k = e_k \quad [7.7]$$

where  $i(k)$  denotes the star  $i$  associated with observation  $k$ , and  $\Delta \mathbf{a}_{i(k)}$  and  $\Delta \mathbf{c}$  denote the column vectors of corrections to the five astrometric parameters and the  $N_c$  calibration parameters respectively.  $\mathbf{B}_k$  and  $\mathbf{C}_k$  denote the row vectors of the derivatives of  $u$  with respect to the astrometric and calibration parameters respectively, divided by  $\sigma_u$ . The  $v_k$  is a centred random variable with unit variance,  $E(v_k) = 0$ ,  $E(v_k^2) = 1$ . The right-hand side is:

$$e_k = \frac{u_{\text{obs}} - u_{\text{calc}}}{\sigma_u} \quad [7.8]$$

In addition to the scheme of weighting in Equation 7.8 some observations were completely rejected, e.g. when the background was very high, or  $|e_k| > 3$ , or  $|u_{\text{obs}} - u_{\text{calc}}| > 1$  arcsec, or when the presence of a parasitic star had been predicted (see Sections 1.6 and 7.2).

---

## 7.2. Processings, Identification, Parasites

---

### Astrometric Processing

The system of observations, given by Equations 7.7, was solved by the least-squares method, giving either astrometric parameters for the stars, or calibration parameters, but not both simultaneously. This means that the right-hand side  $e_k$  in Equation 7.7 was modified by subtracting the 1st or 2nd term on the left-hand side, calculated from the best available parameters, e.g. from a previous solution. The observation equations were used sequentially to update the upper triangular Cholesky factors, which implies that the residuals of a given solution could only be obtained as the right-hand side of the observation equations in a subsequent 'iterated' solution. The numerical method was based on Givens rotations (Lawson & Hanson 1974) thus avoiding the explicit formulation of the normal equations. (Givens rotations also have a very good numerical stability, but this was not important in the present application where the condition number was always small.)

### Sorting of Observations

The astrometric processing received the observations in chronological sequence in the form of 'identified transits'. These included timing and geometric information, the observed signal amplitude and background, and 'parasite' recording', explained below and in Chapter 6. The identified transits could have been used directly as input for the processing, but they were in fact sorted according to the star number of the catalogue. The sorting was carried out for all data from one ESOC tape (high-density 6250 bpi), corresponding to about 24 hours of observation. The purpose of the sorting was to

speed up the processing, i.e. the look-up of the star and its Cholesky factor which could then be updated with all observations for the star obtained during the 24 hours. In retrospect, we believe that the sorting gave only a doubtful advantage, and introduced a considerable complication in the software.

### **Hipparcos Reference Stars**

The observed transits of Hipparcos stars were used as input for all monitoring and calibration purposes, i.e. for provisional solutions of the astrometric parameters, for checking the quality and adequacy of the processing and of the observations.

The star mapper calibration was performed with a subset of about 105 000 stars having accurate positions, parallaxes and proper motions in the intermediate Hipparcos Catalogue, referred to as H30, derived by the two Hipparcos consortia from the first 30 months of observations. This catalogue was rotated to the N18 system derived by NDAC from 18 months of observations because the NDAC attitude was delivered in that system. Thus tying the calibration parameters to a coordinate system defined by Hipparcos positions, parallaxes and proper motions ensured that the resulting five astrometric parameters from Tycho were obtained in the N18 reference system. This catalogue was later rotated and corrected systematically to the final Hipparcos frame, as described in Chapter 11.

The status of Tycho astrometry, including the star mapper calibration after half of the mission was described by Høg *et al.* (1995). The NDAC attitude used by TDAC was given in the N18 system. This caused some problems because it suffered from global systematic differences relative to the H30 system. This inconsistency between the attitude system and the H30 system created global systematic errors in the Tycho reference system which were successfully removed, as described in Chapter 11. It was also realized that Hipparcos parallaxes had to be included in the calibration lest systematic errors would be introduced in the Tycho parallaxes. This explains why the preliminary results discussed by Høg (1995) showed Tycho parallaxes being systematically about 2.0 mas smaller than the Hipparcos values.

The set of astrometric parameters used in prediction updating were the positions from the Tycho Input Catalogue Revision and the proper motions and parallaxes from the Tycho Input Catalogue. The purpose of the astrometric processing was to compute corrections to these values, in the relative tangential coordinate system for each star. The initial 'corrections' were therefore equal to zero. For the Hipparcos reference stars, however, the initial corrections had to be non-zero in order that the stars could act as reference stars for the Tycho Catalogue. The initial corrections for these stars corresponded to the difference in position, parallax and proper motion between Hipparcos (the preliminary catalogue H30 rotated into the NDAC Consortium's intermediate N18 system) and the parameters used in prediction updating. With these values the calibration was carried out, as described in Section 7.3.

In the subsequent computation of astrometric parameters, the initial corrections for the Hipparcos stars were maintained in the iterations of the parallaxes and proper motions, whereas the positions were updated as for all other stars. The reason for not iterating the parallaxes and proper motions for the Hipparcos stars was that the time schedule of the work forbade the required considerable modification of the internal star file. The rather small penalty described in Chapter 18 is that the external standard errors calculated by

comparison with the Hipparcos Catalogue for the parallaxes and proper motions come out as nearly equal to the internal standard errors, which is too small for faint stars.

### **Main Processing and Reprocessing**

The ‘main processing’ treated the 1.3 million stars (entries) contained in the Tycho Input Catalogue Revision. In the main processing, the astrometric solution was iterated many times, using gradually larger data sets, improved values of the attitude and the star mapper calibration, and improved identifications of the transits. The connection to the other tasks in the Hipparcos and Tycho reductions is shown in Figures 1.2 and 10.1.

Following the main processing, a selection of 300 000 stars (see Chapter 10) was reprocessed, with the aim of, amongst others, obtaining improved photometry for the brighter stars, a better detection of double star components and faint stars. Also included were solar system objects. The reprocessing took less time than the main processing because the number of stars was only one tenth of the 3 million in the Tycho Input Catalogue, but the extra complication introduced by having two processings was sizeable.

### **Identification of Transits**

The raw output from the detection process could not be used for astrometric processing due to two error sources both of about 1 arcsec. This size of error was present in the real-time attitude of the satellite and in the positions given in the Tycho Input Catalogue of 3 million stars. The ‘predicted’ transit times (the above ‘calculated’  $\tau_{\text{calc}}$ ) were therefore uncertain by about 2 arcsec, which could disturb the astrometry and photometry too much, as several observed transits might be found within a few arcsec from the predicted time.

This problem was solved by means of the more accurate Tycho Input Catalogue Revision obtained from the first year of Tycho observations (Chapter 5) and the on-ground attitude produced by NDAC for its own use. This catalogue and the attitude were used in an ‘updating’ of all transit times (Chapter 6). The result was a file of ‘identified transits’, which was input for astrometry and photometry calibration and for catalogue production. The astrometric parameters and the calibration were always based on the  $B_T + V_T$  signal since it was demonstrated that the separate use of the  $B_T$  and  $V_T$  signals would give no advantage.

In reality, a PGC Updating-2 (Section 6.1) was used for a provisional identification of transits so that Tycho astrometry and photometry were able to proceed with a test processing, in particular the calibration, without having to wait for the Tycho Input Catalogue Revision. The final Tycho Catalogue is however based on final identified transits from a PGC Updating-3 (Section 6.2).

The transit identification process introduced the data from PGC Updating, and it recorded the possible disturbance from ‘parasitic’ stars as described hereafter.

### **Astrometric Disturbance by Parasitic Stars**

When a star crossed a group of four slits, it generated four peaks in the photon counts. When these counts were folded with the linear digital filter (4-peak filter) described in Chapter 2 the result was a signal with a main lobe and a total of 12 side lobes

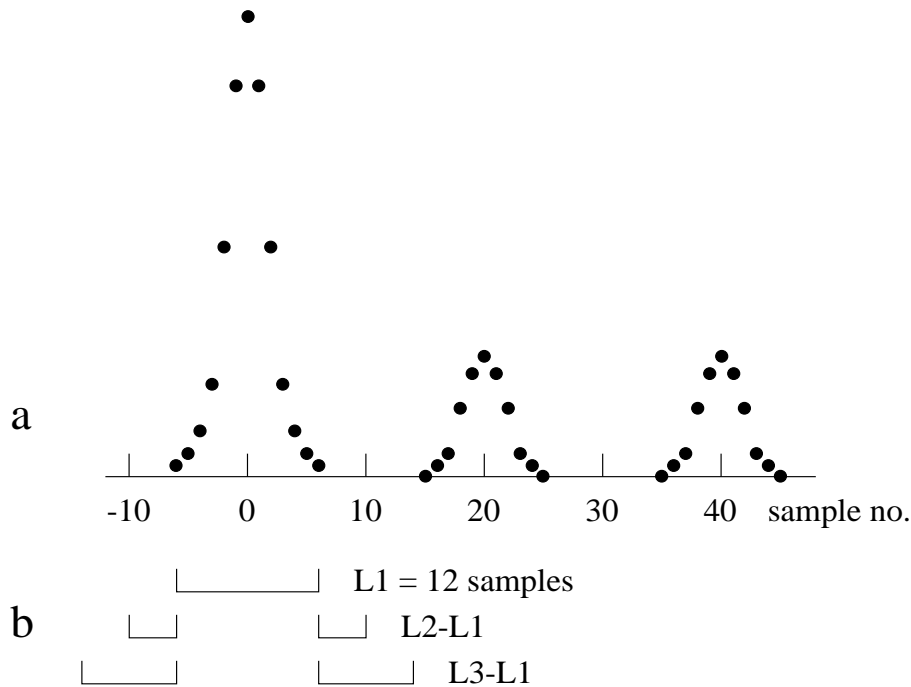


**Figure 7.1.** Strategy for parasite elimination: (a) main lobe and two of the 12 side lobes that would result if the linear filter were used in the detection of transits; the non-linear filter was used thus avoiding the side lobes. (b) An observed transit time of a main lobe was not used for astrometry if a parasite brighter than a certain limiting magnitude was present within certain intervals. A limiting magnitude  $T = 9.9$  mag was applied in a narrow interval  $L1$ , centred on the transit time corresponding to the main lobe. Brighter limits of  $T = 9.4$ ,  $8.9$  mag, respectively, were applied outside, in the intervals  $L2 - L1$  and  $L3 - L1$ , as described in the text.

having one fourth the height of the main lobe (see Figures 2.5 and 7.1). The average separation between lobes was 20 samples equivalent to 5.63 arcsec. In the Tycho detection processing a non-linear filter was used to eliminate the bright side lobes, as illustrated in Figure 2.5. The effect of the side lobes was, however, never completely removed, as was seen from the small excess of double stars with separations of an integer number of 5.63 arcsec (Figure 16.16). A main lobe from one star is called a parasite to another star if it disturbs the main lobe of that star. The added effect of the (main) lobes from several stars in a given interval was recorded for every transit during the transit identification process, where the transit time of all known stars was computed. The added intensity corresponding to the  $B_T + V_T$  signal, called the  $T$  signal, was recorded. In the inner two intervals,  $L1$  and  $L2-L1$ , of Figure 7.1 the  $T$ -magnitude of the parasitic star(s) was taken from the Tycho Input Catalogue Revision. In the outer interval  $L3-L1$ , the intensity was computed from the actual signal estimations in the  $B_T$  and  $V_T$  channels.

The parasite elimination made use of the recorded parasites. In the astrometric analysis, where the identified transits with the recorded parasites were processed, only those transits were used which had no parasites brighter than  $T = 9.9$  mag in the  $L1$ -interval. The limits were  $T = 9.4$  and  $8.9$  mag, respectively in the outer intervals. These limiting magnitudes for parasites have been shown to give a good compromise between rejecting too many transits and accepting too large disturbances.



The astrometric disturbance by parasitic lobes from other stars has been studied by theoretical models. It was shown that there would be 2.7 times as many side lobes of a given magnitude as there are main lobes if a linear filter were used, but this was much diminished by use of the non-linear filter. If nothing had been done to eliminate observations disturbed by the remaining parasitic main lobes, the resulting accuracy would have been significantly impaired, compared to the expectation for pure photon noise. A method was therefore used by which the increase of standard error due to parasites was reduced to a fairly small fraction of the photon noise error. The increase was about 5 per cent at average star density, independent of the stellar magnitude. The fraction increased only slightly to 8 per cent when one of the fields of view was on the galactic equator. If the limiting magnitude for parasites were set 1 mag brighter, the errors would have been increased by about 10 per cent, much more than the 5 per cent with the actual limits.

In the case of double stars the parasites from each star disturbed the other one, thus reducing the number of accepted transits for these stars. A special treatment of narrow double stars was therefore carried out (Chapter 14), where a more thorough analysis was able to avoid an unnecessary loss of transits.

---

### 7.3. Geometric Calibration of the Star Mapper

---

Calibration of the star mapper geometry has been carried out by means of 'identified transits' for 37 months of observations of Hipparcos stars. The results are given in Figures 7.2 and 7.3, for the main processing and the reprocessing. The figures show the numerical effect of each parameter, formally calculated at the ordinate  $z = +10$  arcmin on the grid, as a function of time. Since the parameters are obtained relative to those used by NDAC, Figures 7.2 and 7.3 should be used to discuss only the time variation and the scatter of the parameters.

Each point in the figures is derived from observations obtained over a 24 hour period. The dotted vertical lines mark a refocussing of the telescope which had a pronounced effect on the scale value, and consequently on the shifts  $w_{10}$  and  $w_{20}$ . The reason is that the satellite attitude referred to the centre of the main field of Hipparcos while the vertical slits of the star mapper were located 0.00939 rad or 32 arcmin off-centre.

On theoretical grounds one expects that  $h_{21}^+ \simeq h_{21}^- \simeq 2h_{11}$  and consequently  $h_{21}^+ + h_{21}^- \simeq 4h_{11}$ , but it appears from Figure 7.2 that the time variations of the observed parameter correction obey only the latter relation. It is noted that the time variation of Tycho parameters for, for example, basic angle and rotations cannot be directly compared with the corresponding parameters for the Hipparcos main field because the scale value of the main field is variable with time and this affects the comparison. The corresponding change of scale in the star mapper part is (mainly) absorbed in the shift parameters ( $w_{10}$ ,  $w_{20}$ ,  $h_{-1}$ ,  $h_{+1}$ ), see Figures 7.2 and 7.3.

The scatter of each parameter seen in the figures is about four times the formal standard error, but part of the scatter may be due to a real variation of the parameter. The scatter of points before  $t = 389$  days is somewhat larger than after because the attitude did not have the same quality as after that epoch, as explained in Volume 3, Section 2.1. After the interruption of observations about  $t = 1350$  days the scatter increased.

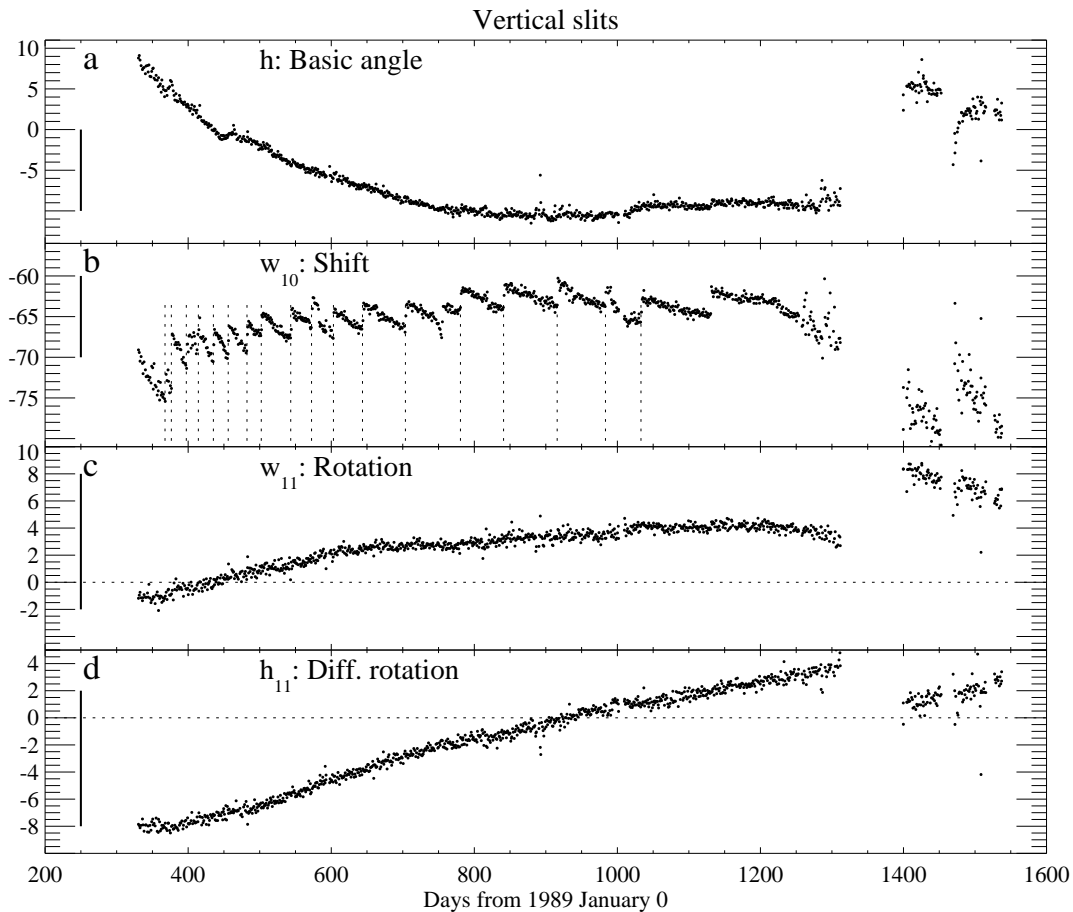


**Figure 7.2.** (a-d) vertical slits, main processing: geometric calibration parameters of the star mapper grid as a function of time. The ordinate, in mas, is the effect of each parameter at the slit coordinate  $z = 10$  arcmin, or actually, the (small) corrections to the parameters used in the prediction and attitude processing. A vertical bar of 10 mas length gives the scale in each plot. Vertical dotted lines in these figures, mark some of the times when the telescope was refocussed (see also Volume 3, Figure 2.1).

The oscillation, in Figures 7.3(f) and 7.3(g), of two parameters for the inclined slits is very conspicuous, with a peak-to-peak amplitude up to 20 mas. This is the same order of magnitude as the attitude uncertainty, but it affects the astrometric parameters more systematically. The problem was related to a small systematic defect in the reprocessing, described in Section 10.7.

It can be seen from Figure 7.2 that the scatter of the parameters during most of the mission produced a combined effect of scatter in Equation 7.2(a-c) of generally less than 1 mas for vertical and 20 mas for inclined slits. For the reprocessing a very similar scatter was found (Figure 7.3). This scatter is negligible compared with photon and attitude noise for the vertical slits, even for the average of, say, eight slit group crossings of a star, sometimes obtained in 24 hours. The 20 mas for the inclined slits is not quite negligible, compared with about 35 mas error of the attitude in the  $z$ -direction. Therefore, a piecewise spline smoothing over four days, excluding discontinuities due

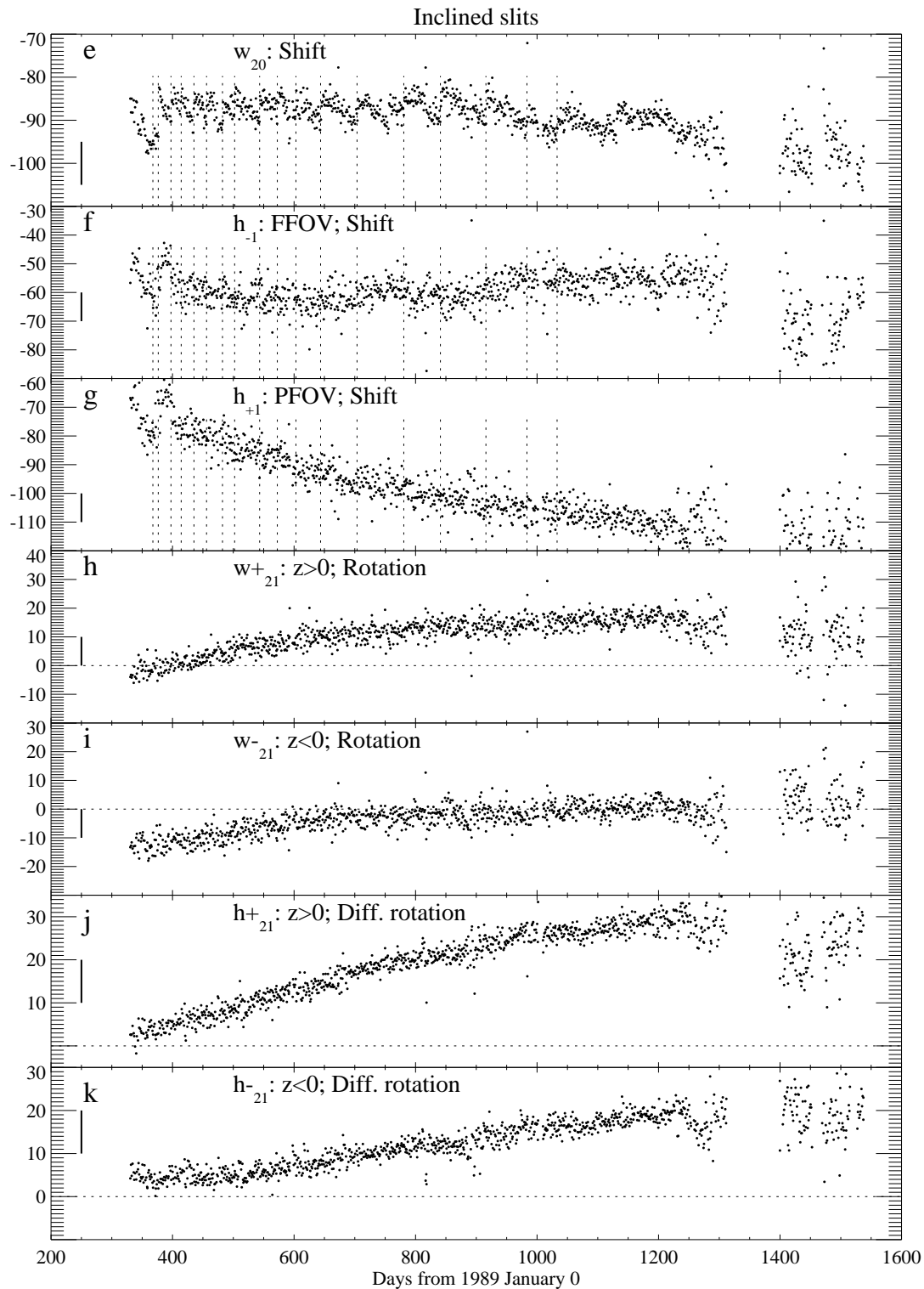


**Figure 7.2. (cont.)** (e-k) inclined slits, main processing: FFOV = following field of view; PFOV = preceding field of view.

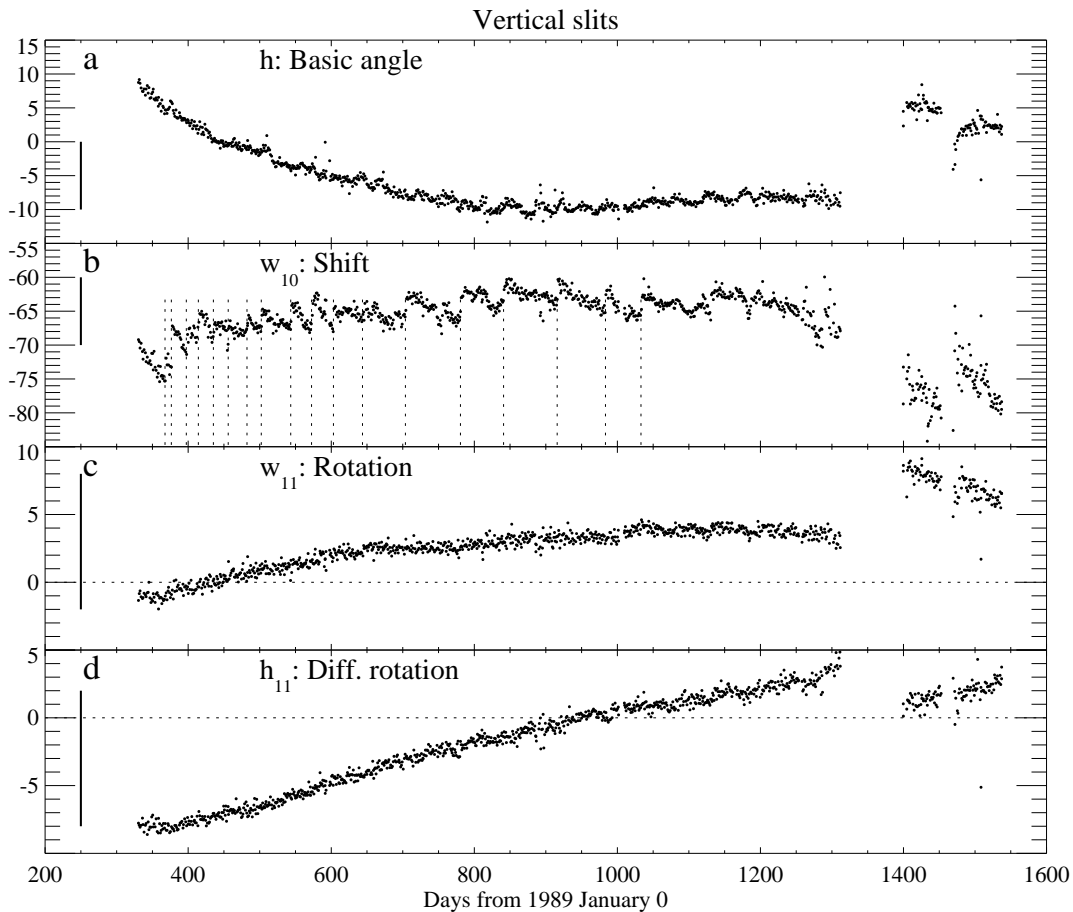


**Figure 7.3.** (a-d) vertical slits, reprocessing: geometric calibration parameters, see Figure 7.2.

to refocussing, was always applied in deriving the parameters used in star catalogue production.

### Medium-Scale Irregularities

The star mapper slits were etched by electron beam scanning on the same glass surface as the main Hipparcos grid. The etching was done one so-called ‘scan field’ at a time before moving the glass plate mechanically to the position required for the next scan field. In this way 68 fields covered the 40 arcmin in  $z$  on the chevron slit group and 34 fields covered the vertical group. The position of the slits in each scan field was measured in the laboratory, resulting in a table of medium-scale irregularities with  $2 \times 68$  values, one for each scan field, as shown in Figure 1.4. These laboratory values of up to 182 mas for the inclined slits were corrected by NDAC using in-orbit data (see Section 1.5), before they were applied in the prediction processing (see Section 4.1). The standard medium-scale irregularities discussed below are therefore corrections to these combined values. The slit errors inside each scan field were shown by laboratory measurements to be negligible. The table of medium-scale irregularities used in the

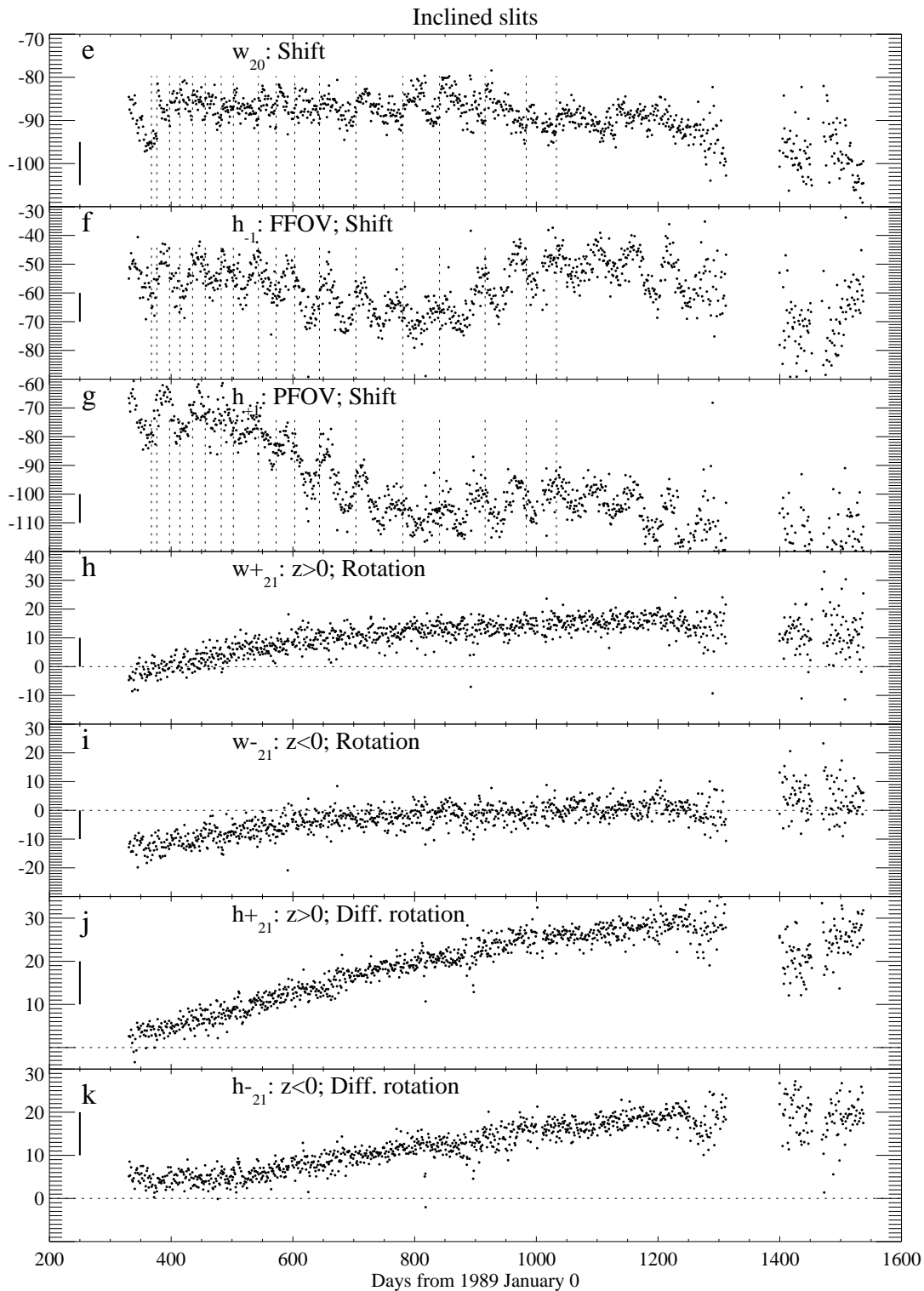


**Figure 7.3. (cont.)** (e-k) inclined slits, reprocessing: geometric calibration parameters, see Figure 7.2. FFOV = following field of view; PFOV = preceding field of view.

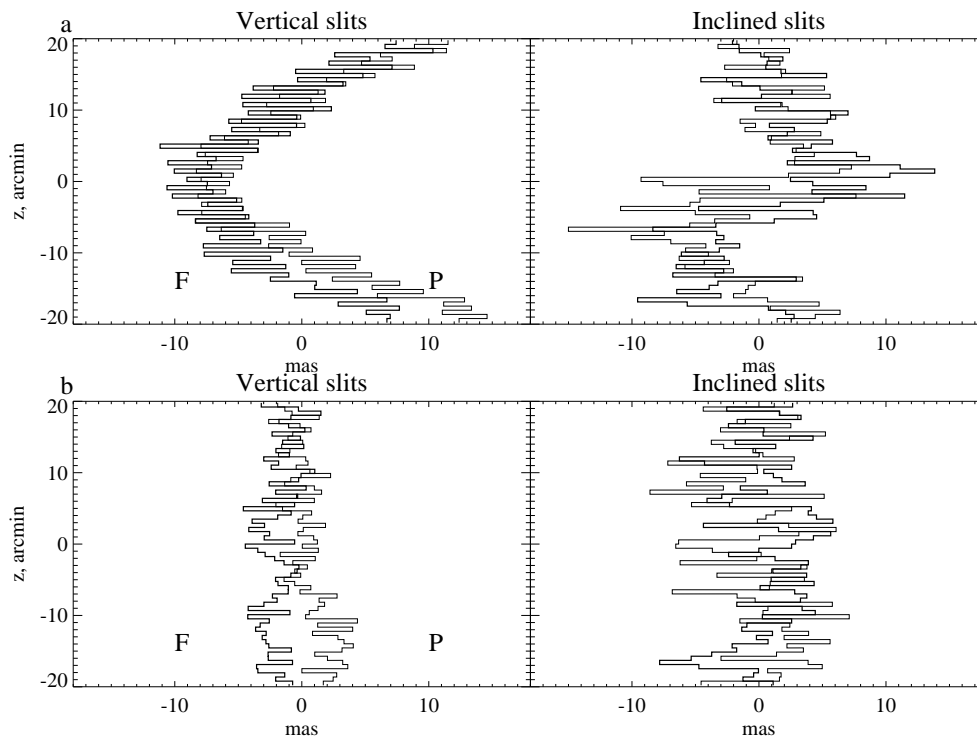


**Figure 7.4.** ‘Medium-scale irregularities’ of the star mapper grid as abscissa and the  $z$ -coordinate as ordinate. Separate values for preceding and following field on the sky are shown by thin and thick lines, marked by  $P$  and  $F$ , respectively. (a) Values determined at the epoch 1991.33; (b) Differences between values obtained at the epochs 1991.33 and 1990.20.

astrometry processing was calculated from residuals in Equation 7.2(a-c) as averages in 68 intervals along  $z$ , corresponding to the distribution of scan fields.

A ‘standard’ table of medium-scale irregularities,  $\Delta w_g(z)$ , was determined from two months of observations at the beginning of the mission and has been used for all calibration and catalogue production. The medium-scale irregularities were verified to be repeatable with another nearby data set within 1 mas systematically, and a scatter per point of 1 and 2 mas for vertical and inclined slits respectively.

Figure 7.4(a) shows the medium-scale irregularities determined for the epoch 1991.33 and for preceding and following fields of view on the sky separately, marked by  $P$  and  $F$ . Hence, it is a figure of  $\Delta w_{fg}(z)$ . A curvature of the vertical slits of 20 mas amplitude appears, and a similar amplitude for inclined slits. The variation between adjacent scan fields is smaller. The lower half of the vertical slits shows a difference about 5 mas between the two fields of view, but this is negligible for Tycho since a star was typically measured in both fields of view within 20 minutes and an average was used for star positions. It was therefore unnecessary to use different medium-scale irregularities for the two fields of view.

Figure 7.4(b) shows the change of medium-scale irregularities during one year of the mission, which appears to be negligible, especially in view of the averaging just mentioned.

---

## 7.4. Astrometric Parameters and Quality Classes

---

The five astrometric parameters for the stars were computed iteratively from the identified transits as described in Section 7.2. The computations produced standard errors, correlation coefficients, an ‘astrometric’ magnitude and various quality indicators for each star. A special file of all, accepted and not accepted, transits was produced for use in the final photometric processing.

### Astrometric Magnitude

An approximate magnitude in the photometric  $T$  channel, with standard error, was computed during one of the early stages of astrometric processing. It was based on the amplitudes given in the identified transits, using photometric calibration parameters received from the Tycho photometric processing. The resulting  $T_a$  magnitude had a considerable bias for faint stars because it was computed from an average of the amplitudes, not by de-censoring. The  $T_a$  magnitude was used for the monitoring of astrometric processing, as illustrated by Figure 7.6, long before the de-censored magnitudes became available. It was also used in the final Tycho Catalogue for 1333 stars, flagged in Field T36 (Section 2.2, Volume 1).

### Hexagon Points

In about 45 000 cases the processing of the first year of Tycho observations did not recognize any star even though the Tycho Input Catalogue contained a rather bright entry of  $< 10.725$  mag. A special effort was therefore made in the astrometric processing to find a star. Six positions were assumed in a regular hexagon with radius 0.6 arcsec, centred on the Tycho Input Catalogue position. A normal astrometric reduction was carried out for the six hexagon points and the Tycho Input Catalogue position. This resulted, after a critical analysis, in 231 further entries in the final Tycho Catalogue; these were often high proper motion stars. In many cases a bright Tycho Input Catalogue entry belonged to a nebula in the Guide Star Catalog used for the Tycho Input Catalogue. (A nebula appears with a considerable diameter and could not be distinguished from a star in the Guide Star Catalog production).

### All-Transits File

In a final astrometric processing an all-transits (AT) file was produced for use in the final photometric processing. The file mainly contained information about the distance of each detection from the final astrometric position of the relevant star, and whether the detection was used for astrometry.

The AT file contained a record for each identified transit with: Tycho star identifier; observation time; amplitude and background in the  $T$  channel; astrometric residual  $\Delta u$ ; standard error  $\sigma_u$ ; and various flags from astrometry. The flags show whether the detection was accepted for astrometry or whether parasites or a large residual were the

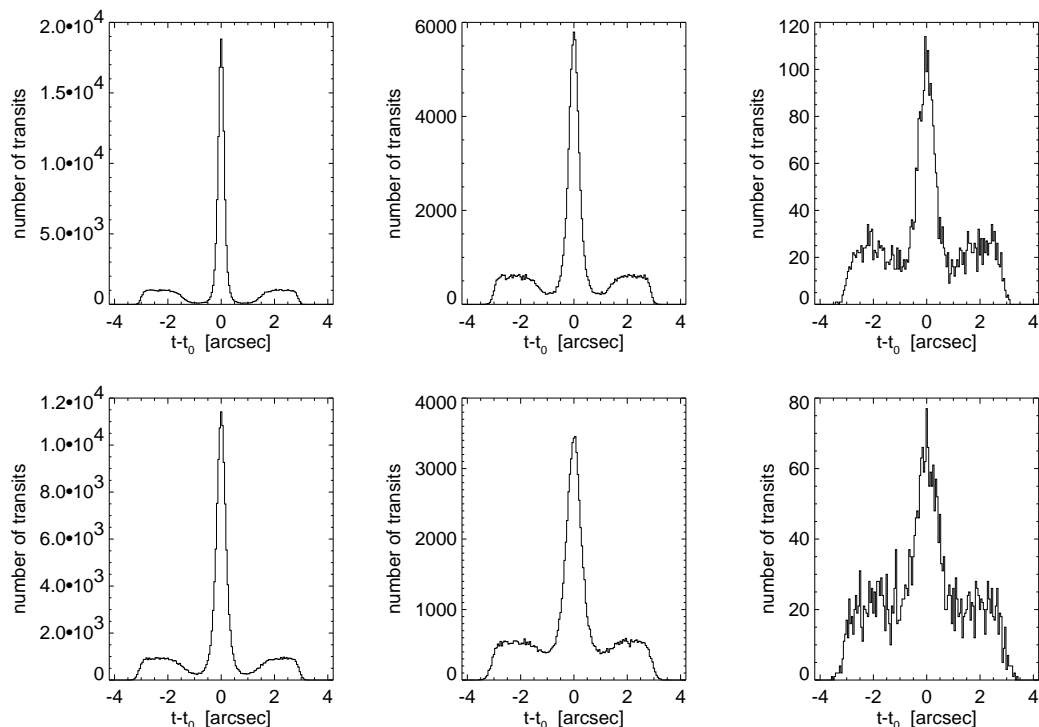


**Figure 7.5.** Accumulated distributions of astrometric residuals for stars with  $H_p$  magnitudes in an interval of 0.2 mag, centred on 9.8, 10.7 and 11.6 mag (left to right); transits on vertical slits in the upper row and on inclined slits in the lower.

reason for a rejection. Some of this information is included in the individual transit records in the Tycho Epoch Photometry Annex, see Volume 1, Table 2.6.2.

### Quality Indicators and Criteria

The standard errors of the five parameters are good quality indicators for the solution for a given star. But they were not sufficient for the present purpose, a reliable distinction of good solutions from bad ones, especially for the faint stars where the single transit could have a signal-to-noise ratio of only 1.5. Special indicators were required to measure the total signal-to-noise ratio of the combined signals from the whole mission in order to distinguish between a real star on the sky and a ‘false’ star, generated by a random accumulation of noise.

The final astrometric quality flag,  $Q$ , is mainly based on the three quality indicators  $\sigma_{\max}$ ,  $F_s$  and  $\sigma_{\text{obsf}}$  (columns 2–4 in Table 7.1).

- The Indicator  $\sigma_{\max}$ : This quantity is the largest of any of the five astrometric standard errors for a given star.
- Signal-to-Noise Ratio,  $F_s$ : This quantity was based on an examination of Figure 7.5 and was computed in a separate processing of all observations after the final astrometric parameters had already been computed.

Figure 7.5 shows the distribution of astrometric residuals,  $\Delta u$ , of Equation 7.5. The central peak in each plot is due to detections from the star, and the residuals outside



**Table 7.1.** The astrometric quality  $Q$  and associated quantities.  $N$  is the number of stars in the Tycho Catalogue of each quality class.  $\sigma_{\text{med}}$  gives the median standard error of a position coordinate at the catalogue epoch J1991.25 (the errors at the mean epoch of observation of any given star are typically 5 per cent smaller).

$Q$	$\sigma_{\text{max}}$ (mas)	$F_s$	$\sigma_{\text{obsf}}$ (mas)	$N$	$\sigma_{\text{med}}$ (mas)	Astrometric quality
1	< 5	> 5	< 300	23147	2.6	very high
2	5 – 10	> 5	< 300	70945	5.5	very high
3	10 – 25	> 5	< 300	259695	13	high
4	25 – 50	> 5	< 300	430182	26	high
5	50 – 150	> 5	< 300	146520	39	medium
6	< 150	> 5	$\geq 300$	41695	44	perhaps non-single
7	< 150	3 – 5	< 300	37821	45	low
8	< 150	3 – 5	$\geq 300$	28949	54	perhaps non-stellar
9	$\equiv 200$	–	–	13077	–	low, ‘R’ in Field T42
$\sqcup$	–	–	–	6301	–	unassigned, ‘H’ in Field T42
any	–	–	–	1058332	25	all entries

an interval from  $-0.7$  to  $+0.7$  arcsec are due to random background detections. The deficit of residuals near the ends of this interval especially for the bright stars is understood from an inspection of the slit response functions in Figure 1.3. A residual about  $0.7$  arcsec would correspond to another star at the foot of the response function where it could, however, not be detected in the presence of the brighter star. For the fainter stars to the right in Figure 7.5 the minimum is less pronounced.

The quantity  $F_s$  is defined as:

$$F_s = (n_1 - n_2) / \sqrt{n_1 + n_2} \quad [7.9]$$

where  $n_1$  is the number of detections within  $0.7$  arcsec along scan from the mean position, and  $n_2$  is the number of detections between  $0.7$  and  $1.4$  arcsec (which provides a measure of the rate of background detections). In the special but rather common case of a sharp image on a negligible background,  $n_1 \sim N_{\text{astrom}}$ ,  $n_2 \sim 0$  and  $F_s \sim \sqrt{N_{\text{astrom}}}$  where  $N_{\text{astrom}}$  is the number of accepted astrometric detections.

- Half-Width of the Image:  $\sigma_{\text{obsf}}$  is the formal standard error of the single observation, being a measure of the half-width of the star image:  $\sigma_{\text{obsf}}^2 = 0.25(\sigma_x^2 + \sigma_y^2)(N_{\text{astrom}} - 5)$ , where  $\sigma_x$  and  $\sigma_y$  are the standard errors of the two position components. A half-width larger than  $300$  mas was found to be correlated with duplicity or a non-stellar image.

### Other Indicators

- Median Standard Error:  $\sigma_{\text{med}}$  is the median standard error of a position coordinate at the catalogue epoch J1991.25. The errors at the mean epoch of observation of any given star are typically 5 per cent smaller.
- Goodness-of-Fit Parameter, F2: This number indicates the goodness-of-fit of the solution to the accepted data. For good fits F2 should approximately follow a normal distribution with zero mean value and unit standard deviation, see Figure 7.6(e). F2 values exceeding  $+2.5$  to  $+3$  thus indicate a bad fit to the data. Its construction and interpretation are explained further under Field H30 in Volume 1, Section 2.1. The

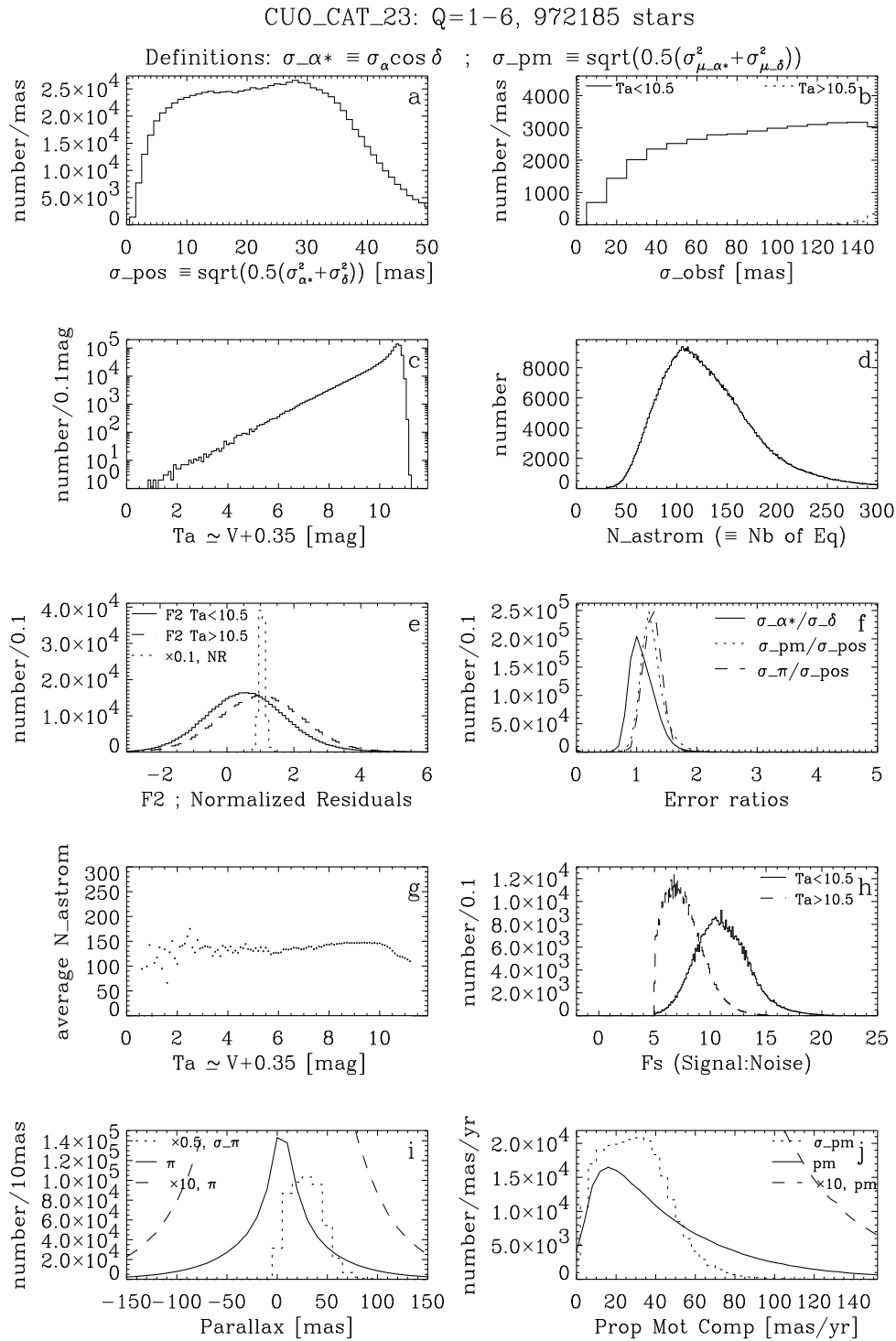


**Figure 7.6.** Distribution functions of quantities derived in the astrometric processing. Such plots for various subsets of the data were extensively used in the quality assessment. The present plot shows as an example the stars with  $Q=1-6$  in one of the intermediate (but nearly final) catalogs, numbered CUO\_CAT\_23.

F2 value was, however, not used for generating the astrometric quality flag  $Q$ , for which classification measures derived from other aspects of the data reduction were found to be more informative.

### Astrometric Quality Flag

The astrometric quality,  $Q$ , is defined for the Tycho data according to Table 7.1, where  $N$  gives the number of stars in the Tycho Catalogue of each quality class. Objects with  $Q \leq 8$  in the Tycho Catalogue all have  $F_s > 3$ ,  $\sigma_{\max} < 150$  mas,  $\sigma_{\text{obsf}} < 450$  mas, and  $N_{\text{astrom}} > 30$ . The last criterion,  $N_{\text{astrom}} \leq 30$ , had only the effect of excluding less than 100 stars of low quality, due to the  $F_s$  limit being the strongest criterion.

Objects with  $Q = 9$  have lower astrometric quality, and are included for the sake of their photometric data—these objects are flagged by ‘R’ in Field T42 (Section 2.2, Volume 1). The last line in the table shows that 6301 entries have ‘H’ in Field T42, showing that they are contained in the Hipparcos Catalogue, but were not observed by Tycho.

A flag is provided (in Field T10) showing if a star is a dubious astrometric reference star, e.g. due to suspected duplicity or dubious astrometry. The remaining approximately 900 000 stars are called ‘recommended astrometric reference stars’.

### Verification of Quality

Development of the quality criteria and their proper combination into astrometric quality classes was a long process where various tools were used. Local sky maps of the actual Tycho catalogue were compared with direct photographs or with the Digitized Sky Survey (DSS). The DSS happened to become available just as needed and it was very extensively used to distinguish stars and nebulae on the sky and compare with entries of various quality classes and false stars. Comparison with the Guide Star Catalog (Version 1.1) was also much used. Pair statistics were used, similar to Figure 16.16. Distribution functions of various quantities were plotted for selected subsets of data as shown by the example in Figure 7.6.

E. Høg

